

ARTICLE

<https://doi.org/10.1038/s41467-019-08835-5>

OPEN

High performance n-type Ag_2Se film on nylon membrane for flexible thermoelectric power generator

Yufei Ding¹, Yang Qiu², Kefeng Cai¹, Qin Yao³, Song Chen⁴, Lidong Chen³ & Jiaqing He²

Researches on flexible thermoelectric materials usually focus on conducting polymers and conducting polymer-based composites; however, it is a great challenge to obtain high thermoelectric properties comparable to inorganic counterparts. Here, we report an n-type Ag_2Se film on flexible nylon membrane with an ultrahigh power factor $\sim 987.4 \pm 104.1 \mu\text{Wm}^{-1}\text{K}^{-2}$ at 300 K and an excellent flexibility (93% of the original electrical conductivity retention after 1000 bending cycles around a 8-mm diameter rod). The flexibility is attributed to a synergetic effect of the nylon membrane and the Ag_2Se film intertwined with numerous high-aspect-ratio Ag_2Se grains. A thermoelectric prototype composed of 4-leg of the Ag_2Se film generates a voltage and a maximum power of 18 mV and 460 nW, respectively, at a temperature difference of 30 K. This work opens opportunities of searching for high performance thermoelectric film for flexible thermoelectric devices.

¹Key Laboratory of Advanced Civil Engineering Materials, Ministry of Education, School of Materials Science and Engineering, Tongji University, 4800 Caoan Road, 201804 Shanghai, China. ²Physics Department, Southern University of Science and Technology, 1088 XueYuan Avenue, 518055 Shenzhen, China. ³State Key Laboratory of High Performance Ceramics and Superfine Microstructure, Shanghai Institute of Ceramics, Chinese Academy of Science, 200050 Shanghai, China. ⁴School of Materials Science and Engineering, Fujian University of Technology, 350108 Fuzhou, China. Correspondence and requests for materials should be addressed to K.C. (email: kfcai@tongji.edu.cn) or to L.C. (email: cld@mail.sic.ac.cn) or to J.H. (email: he.jq@sustc.edu.cn)

Nowadays, the explosive growth of wearable devices has stimulated the development of materials which can power the devices with the energy harvesting from the human body¹. Flexible thermoelectric (TE) materials as the promising energy-harvesting materials, which can directly convert heat into electricity or vice versa and realize the self-power for wearable devices from the temperature difference between the skin and the ambient environment, have attracted increasing attention^{1–8}. The TE performance of a materials is evaluated by the dimensionless figure of merit, $ZT = \alpha^2 \sigma T \kappa^{-1}$, where α , σ , and κ are the Seebeck coefficient, electrical conductivity, and thermal conductivity of the material, respectively, and T is the absolute temperature.

Until now, the research on flexible TE materials mainly focuses on conducting polymers (CPs) and CP-based composite materials^{9–12}; although much progress has been made^{4,13–16}, their ZT values are still incompatible to those of the inorganic TE materials. Moreover, the CP-related materials are mainly p-type while their n-type counterpart is still lacking. For the completion of a high efficiency flexible TE module, high performance of n-type materials are very desirable.

Besides the CPs, insulating polymers are also employed for forming TE composites with inorganic TE materials. For example, most recently, Hou et al.¹⁷ prepared p-type $\text{Bi}_{0.5}\text{Sb}_{1.5}\text{Te}_3$ and epoxy resin composite thick film by hot-pressing (623 K, 4 MPa) and the film shows a high power factor ($\text{PF} = \alpha^2 \sigma$) of $840 \mu\text{W m}^{-1} \text{K}^{-2}$. Recently, flexible substrate, such as polyimide, fiber or paper, has been used to support inorganic materials for preparing high performance and flexible TE materials^{17–22}. For instance, Gao et al.²¹ reported a glass-fiber-aided cold-pressing method for flexible n-type Ag_2Te films on copy paper and the power factor value was up to $85 \mu\text{W m}^{-1} \text{K}^{-2}$ at 300 K. Choi et al.²² prepared n-type HgSe nanocrystal thin film by spin-coating HgSe nanocrystal solution on a plastic substrate and the film showing a maximum power factor of $550 \mu\text{W m}^{-1} \text{K}^{-2}$ at 300 K. Jin et al.²³ deposited Bi_2Te_3 thick film on a cellulose fibers paper via an unbalanced magnetron sputtering technique and the composite film exhibits good flexibility and a power factor of $\sim 250 \mu\text{W m}^{-1} \text{K}^{-2}$ at room temperature.

$\beta\text{-Ag}_2\text{Se}$ is a narrow band semiconductor with an energy gap $E_g = 0.07 \text{ eV}$ at 0 K and it transforms into a cubic superionic conductor ($\alpha\text{-Ag}_2\text{Se}$) around 407 K. $\beta\text{-Ag}_2\text{Se}$, which exhibits high electrical conductivity and low thermal conductivity, has the great potential for n-type TE material near room temperature. Several groups have reported the TE performance of Ag_2Se ^{24–26}. For instance, Ferhat et al.²⁷ prepared $\beta\text{-Ag}_2\text{Se}$ bulks by a direct-reaction of the element Ag and Se in evacuated quartz tubes at 1273 K and the maximum power factor of the material was about $3500 \mu\text{W m}^{-1} \text{K}^{-2}$, which is similar to that of the state-of-art material at room temperature. Most recently, Perez-Taborda et al.²⁸ deposited Ag_2Se films on glass substrates via pulsed hybrid reactive magnetron sputtering and the films showing a high power factor $\sim 2440 \mu\text{W m}^{-1} \text{K}^{-2}$ at room temperature. Nevertheless, the films are with relatively high cost since an expensive facility is used.

Although Ag_2Se materials with excellent TE performance at room temperature have been reported, they are all non-flexible. In this work, we developed a facile strategy to prepare n-type flexible Ag_2Se film on a nylon membrane. The Ag_2Se film showed a very high power factor of $987.4 \mu\text{W m}^{-1} \text{K}^{-2}$ at 300 K, which is one of the best values reported for flexible n-type materials and even comparable to that of some high-ZT inorganic bulk materials at high temperatures, such as SnSe ($\sim 900 \mu\text{W m}^{-1} \text{K}^{-2}$ at 773 K)²⁹ and Cu_{2-x}Se ($1200 \mu\text{W m}^{-1} \text{K}^{-2}$ at 1000 K)³⁰.

Results

Characterization of Ag_2Se film. XRD analysis of the film reveals that all the XRD peaks (Fig. 1a) can be indexed to $\beta\text{-Ag}_2\text{Se}$ phase

(JCPDS No. 24-1041). The XRD peaks for the Ag_2Se film are stronger than those for the Ag_2Se nanowires (NWs) (Supplementary Fig. 3a), and especially the (002) and (004) plane peaks become particularly strong, indicating increase of crystallinity and a large number of the Ag_2Se grains preferentially grown along the (00l) plane³¹. The thickness of the Ag_2Se film is about 10 μm (Supplementary Fig. 5). After hot pressing, the Ag_2Se NWs with diameter of $\sim 65 \text{ nm}$ and length of a few micrometers are sintered into a network-like film with numerous submicron pores (Fig. 1b, c).

To investigate more detailed microstructure of the film, transmission electron microscope (TEM) sample was prepared by FIB and studied by high-angle annular dark field scanning TEM (HAADF-STEM). Figure 1d shows an overview HAADF-STEM image. Although pores ranging from dozens of nanometers to several-hundred nanometers and microgaps indicated by arrows can be observed, generally interior of the film is also dense. Figure 1e shows a typical STEM image. The white dots in Fig. 1e are Pt introduced during the TEM sample preparation. Figure 1f is a FFT pattern corresponding to Fig. 1e. Figure 1g is a typical high-resolution STEM (HRSTEM) image, in which the dot-lines shows grain boundaries, showing well sintered of the Ag_2Se nanograins with different orientations and defects (edge dislocations and stacking faults). XPS analyses (see Supplementary Fig. 6) indicate that the film is stable and no oxidation occurred during the processing.

TE properties of the Ag_2Se film. Figure 2a, b exhibit the TE properties and Hall measurement results of the Ag_2Se film from 300 to 453 K, respectively. The Seebeck coefficient of the film at 300 K is about $-140.7 \mu\text{V K}^{-1}$, indicating n-type conduction. As temperature increases, the absolute Seebeck coefficient shows a decrease tendency and it decreases rapidly when the temperature increases from 393 to 423 K. The electrical conductivity of the film is $\sim 497 \text{ S cm}^{-1}$ at 300 K, and it increases with the temperature increasing from 300 to 393 K and also decreases rapidly when the temperature decreases from 393 to 423 K. The temperature dependence of the Seebeck coefficient and electrical conductivity of the film can be understood from the Hall measurement results (see Fig. 2b), since the Seebeck coefficient is inversely proportional to the power of 2/3 of the carrier concentration⁹ and the electrical conductivity, carrier concentration (n) and carrier mobility (μ) have the relation: $\sigma = ne\mu$.

However, the change tendency above 393 K of the electrical conductivity of the film is not as that for the Ag_2Se film reported in ref. 28, which is mainly because the carrier mobility of our film drops substantially (from ~ 800 to $400 \text{ cm}^2 \text{ V}^{-1} \text{ s}^{-1}$) while that of the latter only drops from ~ 600 to $500 \text{ cm}^2 \text{ V}^{-1} \text{ s}^{-1}$. The temperature dependence of carrier concentration and carrier mobility of the film is similar to that of the bulk Ag_2Se reported in ref. 24, and it suddenly changes around 400 K which is due to the phase transformation from $\beta\text{-Ag}_2\text{Se}$ to $\alpha\text{-Ag}_2\text{Se}$ around 407 K. The carrier concentration first increases with increasing temperature, which is due to thermal excitation of carriers (the concurrent decrease in the Seebeck coefficient of the film suggests that the additional carriers are holes). When the temperature is beyond the phase transition temperature (407 K), the Ag_2Se becomes a superionic conductor, and then the carrier concentration almost keeps constant. The mobility suddenly drops significantly across the superionic transition, the reason for which is that the Ag ions in superionic Ag_2Se move freely and tend to scatter electrons more efficiently than a static lattice²⁴.

As a result, as the temperature increases, the power factor value also shows a similar change tendency to that of electrical conductivity: increases from 987.4 at 300 K to $1448.1 \mu\text{W m}^{-1} \text{K}^{-2}$ at 393 K, then rapidly decreases to $569.2 \mu\text{W m}^{-1} \text{K}^{-2}$ at $\sim 423 \text{ K}$.

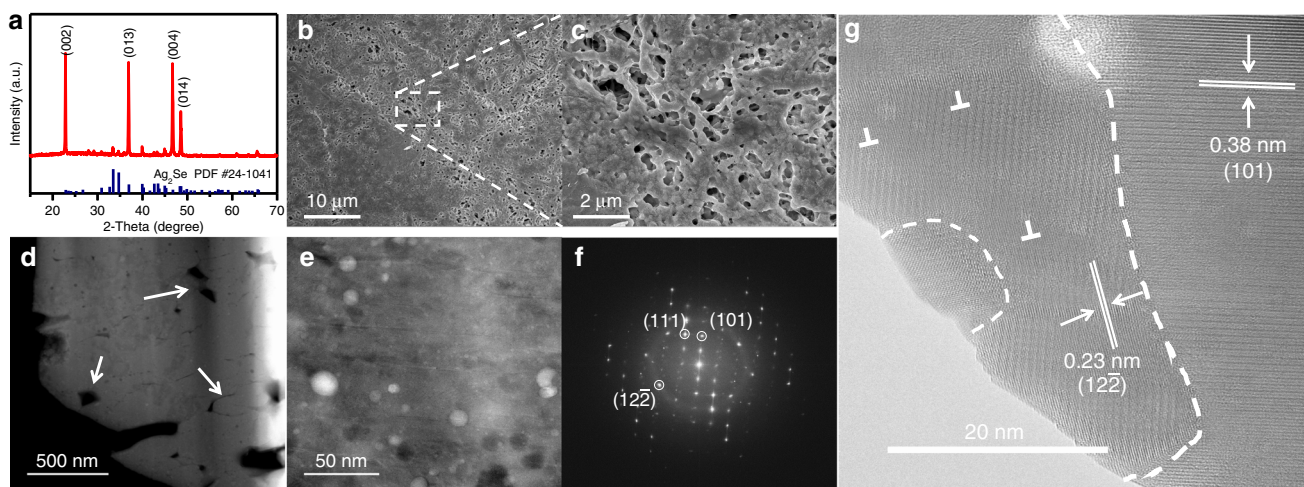


Fig. 1 Characterization of the Ag_2Se film. **a** XRD pattern of the Ag_2Se film. **b** Low magnification surface FESEM image of the Ag_2Se film. **c** High magnification surface FESEM image of the Ag_2Se film. **d** Overview HAADF-STEM image. **e** Typical STEM image. **f** FFT image corresponding to **e**. **g** Typical HRSTEM image

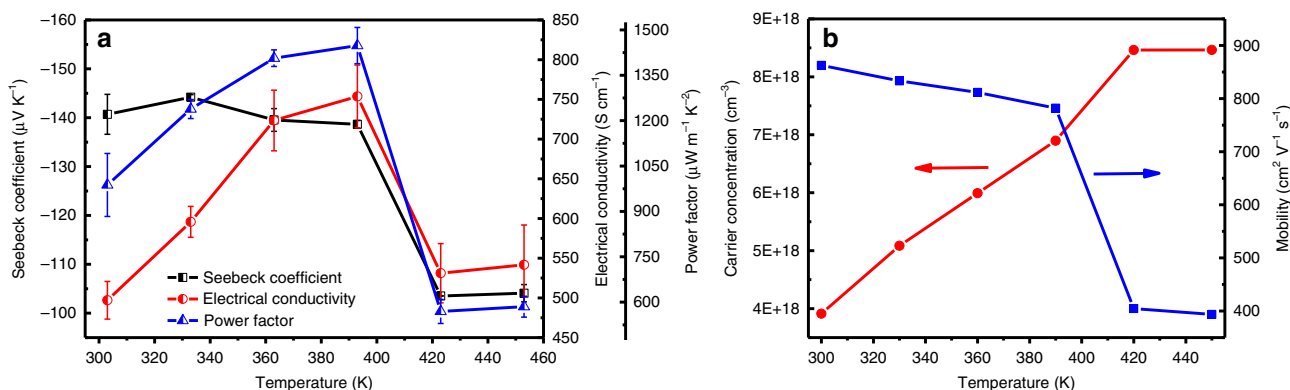


Fig. 2 In-plane TE properties of the film. **a** Temperature dependence of Seebeck coefficient, electrical conductivity and power factor for the Ag_2Se film (Each point shows the standard deviations from two independent measurements). **b** Temperature dependence of carrier concentration and mobility for the Ag_2Se film

The power factor value at 300 K is among the best n-type flexible TE materials (See Table 1). However, it is still much lower than the best value of the bulk Ag_2Se with optimal carrier concentration reported in ref.²⁷. In order to understand the mechanism, we hot pressed a bulk sample without nylon. The bulk sample, with similar relative density and its grains without preferential growth direction (see Supplementary Fig. 8), has a power factor of $\sim 1340 \mu\text{W m}^{-1} \text{K}^{-2}$ at room temperature (see Supplementary Fig. 9). Hence, we deduce that the main reasons for the film with lower power factor are: the film with high porosity, its grains preferentially grown along (00*l*), and its carrier concentration not optimized.

As it is hardly to separate the Ag_2Se film from the nylon membrane without destroy the film, the in-plane thermal conductivity of the Ag_2Se film cannot be provided here (the in-plane thermal conductivity of the Ag_2Se film on nylon membrane was measured to be $0.449 \text{ W m}^{-1} \text{K}^{-1}$, see Supplementary Table 1). However, it is deduced as follows: A $\kappa_e (=L\sigma T)$ of $0.268 \text{ W m}^{-1} \text{K}^{-1}$ is estimated for our film by using the same Lorenz number ($L = 1.8 \times 10^{-8} \text{ W}\Omega\text{K}^{-2}$) as used in ref.²⁸. As our Ag_2Se film contains pores with sizes ranging from $\sim 20 \text{ nm}$ to submicrometers (see Supplementary Fig. 7 and Fig. 1c), nanograins (see Fig. 1g) and a

hetero-interface between the Ag_2Se film and nylon membrane (see Fig. 3b and Supplementary Fig. 5), disorder in terms of nanocrystallite boundaries, microstructural defects (dislocations and amorphous regions), heat-carrying phonons in a wide spectrum of wavelengths can be scattered. The microstructural defects, such as dislocations (a few nm) and heterointerfaces, are effective in scattering the short wavelength phonons, and the nanocrystallite boundaries and residual nanopores ($\sim 20\text{--}200 \text{ nm}$) play an effective role in scattering the mid-to-high wavelength phonons^{32–34}, thus the lattice contribution κ_l will be lower than that ($\kappa_l \sim 0.21 \text{ W m}^{-1} \text{K}^{-1}$) of the Ag_2Se film consisting of micrograins in ref. 28, which suggests that the in-plane thermal conductivity ($\kappa_e + \kappa_l$) of our film will be lower than $0.478 \text{ W m}^{-1} \text{K}^{-1}$. Hence, the ZT value at 300 K of our film is estimated to be ~ 0.6 .

The TE properties of a $\beta\text{-Ag}_2\text{Se}$ single crystal from 160 to 300 K are calculated using the first-principle density functional theory (see details in Supplementary Fig. 10 and Supplementary Note 5)³⁵. The calculation shows that the power factor along the b-axis ((0*l*0) direction) is about $2465 \mu\text{W m}^{-1} \text{K}^{-2}$ at 300 K, which is about two orders of magnitude higher than that along other two axes. Recall that the present film is preferentially grown along (00*l*) direction (see Fig. 1a) and we hereinbefore deduced that the Ag_2Se grains

Table 1 Comparison of TE performance of flexible n-type TE materials at room temperature

Materials	α ($\mu\text{V K}^{-1}$)	σ (S cm^{-1})	PF ($\mu\text{W m}^{-1} \text{K}^{-2}$)	Ref.
Ag ₂ Te/copy-paper	-100	85	85	21
Cu-doped Bi ₂ Se ₃ /PVDF	-84	146	103.2	43
Ni NWs/PVDF	-20.6	4700	200	44
Bi ₂ Te ₃ /Cellulose fiber	-130	148	250	23
C ₆₀ /TiS ₂	-101	390	400	40
HgSe	-518	20	550	22
TiS ₂ [tetrabutylammonium] _{0.013} [hexylammonium] _{0.019}	-150	400	904	45
Ag ₂ Se/Nylon membrane	-140	497	987	This work

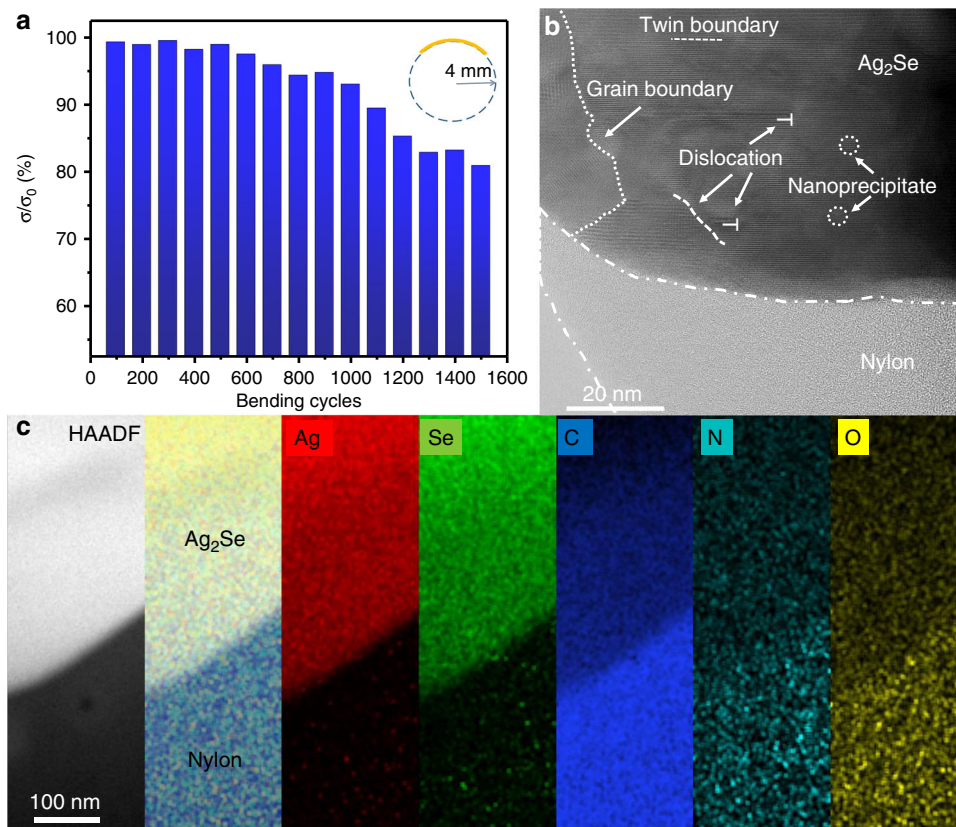


Fig. 3 Flexibility of the film and evaluation of the heterointerface. **a** The ratio of electrical conductivity of the film before and after bending as a function of bending cycles. **b** HRSTEM image showing good combination between the Ag₂Se film and nylon membrane. **c** From left to right: HAADF image of a heterointerface between a Ag₂Se grain and nylon, overall corresponding EDS image and EDS image of elemental Ag, Se, C, N, and O

grown along (001) direction is not good to TE properties, which agrees with the calculation results. This implies that the TE properties of our Ag₂Se film can be further improved via tuning the orientation of the Ag₂Se grains, increasing the density and optimizing the carrier concentration.

Flexibility of the Ag₂Se film. In order to test the flexibility of the Ag₂Se film, a bending test was applied around a rod with a diameter of 8 mm. Figure 3a demonstrates the ratio (σ/σ_0) of the electrical conductivity with or without bending with different cycles. The electrical conductivity decreases slowly with the increasing of bending cycles. About 93 and 80% of the initial electrical conductivity are maintained after 1000 and 1500 bending cycles, respectively. Compared with the n-type Ag₂Te films on copy paper²¹, the n-type Bi₂Te₃ thick film on a cellulose

fibers paper²³, and p-type PEDOT/Bi₂Te₃ hybrid films with monodispersed and periodic Bi₂Te₃ nanophase fabricated via a very complicated process¹⁶, our Ag₂Se film on nylon membrane shows a better flexibility (see Supplementary Table 2).

In order to better understand the excellent flexibility of the film. We deliberately examined the details near the interface between the Ag₂Se film and the nylon membrane. We found that the Ag₂Se grains are well combined with the amorphous nylon membrane (Fig. 3b), indicating that there is a good bonding between them, resulted from the hot pressing, which is good for flexibility²¹. In Fig. 3c, from left to right is a HAADF-STEM image near a heterointerface, overall corresponding EDS image, elemental EDS images of Ag, Se, C, N, and O, respectively. The elements of C, N, and O are attributed to the CONH group of the nylon. It is seen from the EDS images of elemental Ag and Se that

a small amount of these two elements are detected in the nylon membrane. This is because the nylon membrane is porous (pore size ~ 200 nm), and some tips of the Ag_2Se nanowires may penetrate into the pores during the filtration and they bonded together during the hot pressing.

Therefore, the good flexibility of the Ag_2Se film on nylon membrane can be explained by the following reasons. Firstly, as known to all, nylon has an intrinsic excellent flexibility. Secondly, the Ag_2Se film is in fact a porous network intertwined with numerous Ag_2Se nanograins sintered from large aspect ratio of Ag_2Se nanowires; porous structure can accommodate the bending of the film³⁶, hence, the film itself should have a certain flexibility. Moreover, the nylon membrane and the Ag_2Se film have a good bonding (see Fig. 3b, c). In addition, most recently, Shi et al.³⁷ reported that Ag_2S semiconductor exhibits an extraordinary metal-like ductility with high plastic deformation strains at room temperature. As Se and S are in the same family, Ag_2Se may have a similar ductility.

Device performance. As shown in Fig. 4a, the TE prototype device consists of 4 pieces of the film. Each leg is 5 mm in width and 20 mm in length. To decrease the contact resistance between the film and silver paste^{38,39}, gold was first evaporated on two ends of each leg and then silver paste was painted to connect the legs in series. The open-circuit voltage and output power were measured with a homemade apparatus (see Supplementary Fig. 11 and Supplementary Note 6). Figure 4b shows the relationship between the open-circuit voltage and temperature difference. The open-circuit voltage is proportional to the temperature difference. When the temperature difference is 30 K, the measured open-circuit voltage is about 18 mV. And the calculated open-circuit voltage can be estimated by the expression of $U_{oc} = N \cdot |\alpha| \cdot \Delta T$ (N is the number of legs). In this case, $|\alpha|$ is about $143 \mu\text{V K}^{-1}$, thus the U_{oc} ($=4 \times 143 \times 10^{-3} \times 30$) is about 17.2 mV, which is quite close to the measured one (the difference may be resulted from the error of the temperature (± 1 K) during the measurement). The output power (P) is calculated by the equation as follows:

$$P = I^2 R_{load} = \left(\frac{U_{oc}}{R_{in} + R_{load}} \right)^2 R_{load} \quad (1)$$

where I is the output current, R_{load} is the load resistance and R_{in} is the internal resistance of the device.

The curve of output voltage—current and that of output power—current are shown in Fig. 4c. The output voltage is inversely proportional to output current. At the temperature difference of 30 K, the measured maximum output power is about 460 nW. According to Eq. (1), when the load resistance (R_{load}) equals to the internal resistance (R_{in}) of the device, the maximum output power is obtained. And the load resistance which can be calculated from the Fig. 4c is about 250Ω (the voltage is about 10.7 mV and the current is about $42.9 \mu\text{A}$), matches the measurement of the internal resistance of the device. The maximum power density is about 2.3 W m^{-2} , obtained from dividing the power by the cross-sectional area and the number of legs¹⁸, which is somewhat higher than that of reported flexible n-type devices^{40–42}, confirming that the Ag_2Se film possesses high TE performance.

Discussion

In summary, we used a simple and low cost process compared with other published methods, i.e., first synthesis of Ag_2Se nanowires then vacuum assisted filtration on nylon membrane and finally hot pressing at a relatively low temperature, to endow the film starting from the Ag_2Se nanowires both good TE

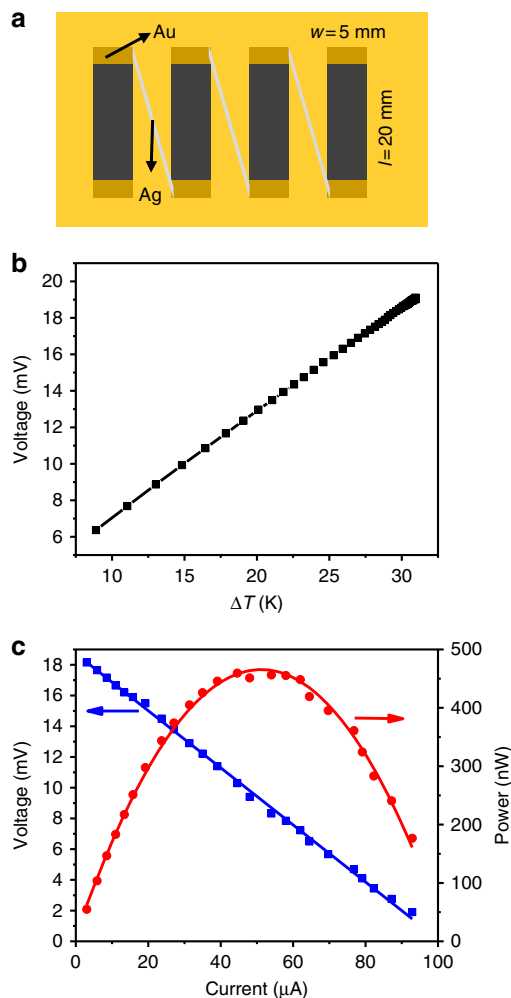


Fig. 4 Schematic illustration and performance of the prepared device. **a** The schematic illustration of the TE device. **b** The open-circuit voltage at various temperature difference. **c** The output voltage and output power versus current at temperature difference of 30 K

properties and excellent flexibility. A high power factor of $987.4 \pm 104.1 \mu\text{W m}^{-1} \text{K}^{-2}$ at 300 K was obtained, which is a record value among the recently reported n-type flexible TE materials. The high power factor comes from the special Ag_2Se film; and the excellent flexibility comes from the nylon membrane, the porous nanostructured Ag_2Se film, and good combination of the Ag_2Se film and nylon membrane. A prototype device with 4-leg of the film connected with silver paste was fabricated. The maximum power density of the device is about 2.3 W m^{-2} at a temperature difference of 30 K. Together with the good TE properties of the Ag_2Se film and excellent flexibility of the nylon membrane, the Ag_2Se film on nylon membrane has shown great promise in flexible TE modules for wearable energy harvesting. This work demonstrates an effective route to fabricate high-performance flexible TE films.

Methods

Synthesis. The Ag_2Se film was prepared by a vacuum-assisted filtration of a Ag_2Se -nanowire dispersion on a porous nylon membrane and the film on the nylon membrane was dried at 60°C in vacuum overnight and then hot-pressed at 200°C and 1 MPa for 30 min. See details in Supplementary Figs. 1–4 and Supplementary Note 1–2. The bulk Ag_2Se was hot-pressed at 200°C and 24 MPa for 30 min for comparison (Supplementary Note 3).

Characterization. The phase composition of the Ag_2Se film was examined by X-ray diffraction (XRD) using $\text{Cu K}\alpha$ radiation (D/MAX 2550VB3+/PCII). The

morphology of the film was observed by a field emission scanning electron microscope (FESEM, FEI Nova NanoSEM 450). The internal microstructure of the film was examined by double-aberration corrected transmission electron microscope (TEM, FEI Titan @300 kV in TEM and STEM mode), and the TEM sample was prepared by the Focused Ion Beam (FIB, FEI Helios600i) with the in-situ lift-out technique. To protect the sample surface before the ion milling, a Pt layer was sputtered on the full sample. The region of interest was further locally capped in the FIB with ion beam deposited carbon. The major milling was done with a 30 kV Ga ion beam while the milling progress was controlled with the scanning electron microscope. Final milling to minimize the damage layer on the specimen was performed with 5 kV followed by 2 kV Ga ion beam. X-ray photoelectron spectroscopy (XPS, ESCALAB 250Xi) was used to examine the bonding energy of the film. The pore distribution and pore volume were measured by a Brunauer-Emmett-Teller (BET) analyzer (Micromeritics, ASAP 2020).

Measurement of TE properties and performance. The in-plane electrical conductivity and Seebeck coefficient were measured by the standard four-probe method (Sinkuriko, ZEM-3) in He atmosphere. The in-plane thermal conductivity was calculated by $\kappa = \rho \cdot D \cdot C_p$, where ρ , D , and C_p are the density, thermal diffusivity, and specific heat capacity, respectively. The in-plane D was measured by the laser flash method (LFA467, NETZSCH), C_p was measured by the differential scanning calorimetry (DSC Q2000, TA), and the ρ was obtained by measuring the mass and geometrical dimensions of the film with nylon (Supplementary Note 4). The Hall coefficient was measured by the Hall measurement system (LakeShore 8404). The measurement error for σ and α is about $\pm 5\%$. The thickness of the films was determined by a thickness meter (Shanghai Liu Ling Instrument Factory) combined with FESEM observation. The bending test of the film was performed using a homemade apparatus around a rod with a diameter of 8 mm.

The film was cut into strips (20 mm \times 5 mm), and the strips were pasted on a polyimide substrate (the interval of two strips is ~ 5 mm). The two ends of each strip were coated with a layer of Au via a mask and evaporation. After that, each strip was connected in series with Ag paste as conductive connection to obtain a prototype power generator. The output voltage and output power of the device were measured by a homemade apparatus (see Supplementary Fig. 11 and Supplementary Note 6).

Data availability

The data that support the findings of this study are available from the corresponding author upon reasonable request.

Received: 31 August 2018 Accepted: 1 February 2019

Published online: 19 February 2019

References

- Bahk, J., Fang, H. & Shakouri, A. Flexible thermoelectric materials and device optimization for wearable energy harvesting. *J. Mater. Chem. C* **3**, 10362–10374 (2015).
- Bharti, M., Singh, A., Samanta, S. & Aswal, D. K. Progress in materials science conductive polymers for thermoelectric power generation. *Prog. Mater. Sci.* **93**, 270–310 (2018).
- Zhang, L. et al. Fiber-based thermoelectric generators: materials, device structures, fabrication, characterization, and applications. *Adv. Energy Mater.* **8**, 1700524 (2017).
- Park, T., Park, C., Kim, B., Shin, H. & Kim, E. Flexible PEDOT electrodes with large thermoelectric power factors to generate electricity by the touch of fingertips. *Energy Environ. Sci.* **6**, 788–792 (2013).
- Kim, S. J., We, J. H. & Cho, B. J. A wearable thermoelectric generator fabricated on a glass fabric. *Energy Environ. Sci.* **7**, 1959–1965 (2014).
- Du, Y. et al. Thermoelectric fabrics: toward power generating clothing. *Sci. Rep.* **5**, 6411 (2015).
- Bae, E. J., Kang, Y. H., Jang, K. & Cho, S. Y. Enhancement of thermoelectric properties of PEDOT: PSS and tellurium-PEDOT: PSS hybrid composites by simple chemical treatment. *Sci. Rep.* **6**, 18805 (2016).
- Song, H. & Cai, K. Preparation and properties of PEDOT:PSS/Te nanorod composite films for flexible thermoelectric power generator. *Energy* **125**, 519–525 (2017).
- Snyder, G. J. & Toberer, E. S. Complex thermoelectric materials. *Nat. Mater.* **7**, 105–114 (2008).
- Du, Y., Shen, S. Z., Cai, K. & Casey, P. S. Research progress on polymer-inorganic thermoelectric nanocomposite materials. *Prog. Polym. Sci.* **37**, 820–841 (2012).
- Zhang, Q., Sun, Y., Xu, W. & Zhu, D. Organic thermoelectric materials: emerging green energy materials converting heat to electricity directly and efficiently. *Adv. Mater.* **26**, 6829–6851 (2014).
- Gayner, C. & Kar, K. K. Progress in materials science recent advances in thermoelectric materials. *Prog. Mater. Sci.* **83**, 330–382 (2016).
- Bubnova, O. et al. Optimization of the thermoelectric figure of merit in the conducting polymer poly(3,4-ethylenedioxythiophene). *Nat. Mater.* **10**, 429–433 (2011).
- Wang, H. et al. Thermally driven large n-type voltage responses from hybrids of carbon nanotubes and Poly(3,4-ethylenedioxythiophene) with tetrakis(dimethylamino) ethylene. *Adv. Mater.* **27**, 6855–6861 (2015).
- Fan, Z., Du, D., Guan, X. & Ouyang, J. Polymer films with ultrahigh thermoelectric properties arising from significant seebeck coefficient enhancement by ion accumulation on surface. *Nano Energy* **51**, 481–488 (2018).
- Wang, L., Zhang, Z., Liu, Y., Wang, B. & Wang, S. Exceptional thermoelectric properties of flexible organic-inorganic hybrids with monodispersed and periodic nanophase. *Nat. Commun.* **9**, 3817 (2018).
- Hou, W. et al. Fabrication and excellent performances of Bi_{0.5}Sb_{1.5}Te₃/epoxy flexible thermoelectric cooling devices. *Nano Energy* **50**, 766–776 (2018).
- Finefrock, S., Zhu, X., Suna, Y. & Wu, Y. Flexible prototype thermoelectric devices based on Ag₂Te and PEDOT:PSS coated nylon fibre. *Nanoscale* **7**, 5598–5602 (2015).
- Sun, C., Goharpey, A. H., Rai, A., Zhang, T. & Ko, D. Paper thermoelectrics: merging nanotechnology with naturally abundant fibrous material. *ACS Appl. Mater. Interfaces* **8**, 22182–22189 (2016).
- Rojas, J. P., Conchouso, D., Arevalo, A. & Singh, D. Paper-based origami flexible and foldable thermoelectric nanogenerator. *Nano Energy* **31**, 296–301 (2017).
- Gao, J. et al. A novel glass-fiber-aided cold-press method for fabrication of n-type Ag₂Te nanowires. *J. Mater. Chem. A* **5**, 24740–24748 (2017).
- Choi, J. et al. Large voltage generation of flexible thermoelectric nanocrystal thin films by finger contact. *Adv. Energy Mater.* **7**, 1700972 (2017).
- Jin, Q. et al. Cellulose fiber-based hierarchical porous bismuth telluride for high-performance flexible and tailorable thermoelectrics. *ACS Appl. Mater. Interfaces* **10**, 1743–1751 (2018).
- Day, T. et al. Evaluating the potential for high thermoelectric efficiency of silver selenide. *J. Mater. Chem. C* **1**, 7568–7573 (2013).
- Pei, J. et al. Rapid synthesis of Ag₂Se dendrites with enhanced electrical performance by microwave-assisted solution method. *New J. Chem.* **37**, 323–328 (2013).
- Yang, D., Su, X., Meng, F., Wang, S. & Yan, Y. Facile room temperature solventless synthesis of high thermoelectric performance Ag₂Se via a dissociative adsorption reaction. *J. Mater. Chem. A* **5**, 23243–23251 (2017).
- Ferhat, M. & Nagao, J. Thermoelectric and transport properties of β -Ag₂Se compounds. *J. Appl. Phys.* **88**, 813–816 (2000).
- Perez-taborda, J. A., Caballero-calero, O., Vera-londono, L., Briones, F. & Martin-gonzalez, M. High thermoelectric zT in n-type silver selenide films at room temperature. *Adv. Energy Mater.* **8**, 1702024 (2018).
- Chang, C. et al. 3D charge and 2D phonon transports leading to high out-of-plane ZT in n-type SnSe crystals. *Science* **360**, 778–783 (2018).
- Liu, H. et al. Copper ion liquid-like thermoelectrics. *Nat. Mater.* **11**, 422–425 (2012).
- Mu, X. et al. Enhanced electrical properties of stoichiometric Bi_{0.5}Sb_{1.5}Te₃ film with high-crystallinity via layer-by-layer in-situ Growth. *Nano Energy* **33**, 55–64 (2017).
- Bux, B. S. K. et al. Nanostructured bulk silicon as an effective thermoelectric material. *Adv. Funct. Mater.* **19**, 2445–2452 (2009).
- Bathula, S. et al. Enhanced thermoelectric figure-of-merit in spark plasma sintered nanostructured n-type SiGe alloys. *Appl. Phys. Lett.* **101**, 213902 (2012).
- Zhu, G. H. et al. Increased phonon scattering by nanograins and point defects in nanostructured silicon with a low concentration of germanium. *Phys. Rev. Lett.* **102**, 196803 (2009).
- Fang, C. M., Groot, R. A., De & Wieggers, G. A. Ab initio band structure calculations of the low-temperature phases. *J. Phys. Chem. Solids* **63**, 457–464 (2002).
- Yang, W. et al. Large-deformation and high-strength amorphous porous carbon nanospheres. *Sci. Rep.* **6**, 24187 (2016).
- Shi, X. et al. Room-temperature ductile inorganic semiconductor. *Nat. Mater.* **17**, 421–426 (2018).
- Song, H. et al. Polymer/carbon nanotube composite materials for flexible thermoelectric power generator. *Compos. Sci. Technol.* **153**, 71–83 (2017).
- He, R., Schiering, G. & Nielsch, K. Thermoelectric devices: a review of devices, architectures, and contact optimization. *Adv. Mater. Technol.* **3**, 1700256 (2018).
- Wang, L. et al. Solution-printable fullerene/TiS₂ organic/inorganic hybrids for high-performance flexible n-type thermoelectrics. *Energy Environ. Sci.* **11**, 1307–1317 (2018).

41. Wan, C. et al. Flexible n-type thermoelectric materials by organic intercalation of layered transition metal dichalcogenide TiS_2 . *Nat. Mater.* **14**, 622–627 (2015).
42. Liu, L. et al. Flexible unipolar thermoelectric devices based on patterned poly $[\text{K}_x(\text{Ni-ethylenetetrahiolate})]$ thin films. *Mater. Chem. Front.* **1**, 2111–2116 (2017).
43. Dun, C. et al. Flexible n-type thermoelectric films based on Cu-doped Bi_2Se_3 nanoplate and Polyvinylidene Fluoride composite with decoupled Seebeck coefficient and electrical conductivity. *Nano Energy* **18**, 306–314 (2015).
44. Chen, Y. et al. Bendable n-type metallic nanocomposites with large thermoelectric power factor. *Adv. Mater.* **29**, 1604752 (2017).
45. Wan, C. et al. Ultrahigh thermoelectric power factor in flexible hybrid inorganic-organic superlattice. *Nat. Commun.* **8**, 1024 (2017).

Acknowledgements

This work was supported by the Key Program of National Natural Science Foundation of China (51632010 and 51632005), National Basic Research Program of China (973 Program) under Grant No. 2013CB632500, the foundation of the State Key Lab of Advanced Technology for Material Synthesis and Processing (Wuhan University of Technology), and Innovation Commission of Shenzhen Municipality (Grant Nos. KQTD2016022619565991 and KQCX2015033110182370).

Author contributions

Y.D. and K.C. conceived the idea, discussed and analyzed the data. Y.D. performed the majority of experiments and drafted the manuscript; K.C. designed the whole work and revised the manuscript; Y.Q. and J.H. prepared the TEM sample and analyzed the microstructure by STEM; Q.Y. and L.C. contributed the thermoelectric properties measurement; L.C. proposed valuable advice for revising the manuscript. S.C. contributed the theoretical calculation. All authors discussed the results and commented on the manuscript.

Additional information

Supplementary Information accompanies this paper at <https://doi.org/10.1038/s41467-019-08835-5>.

Competing interests: The authors declare no competing interests.

Reprints and permission information is available online at <http://npg.nature.com/reprintsandpermissions/>

Journal peer review information: *Nature Communications* thanks the anonymous reviewers for their contribution to the peer review of this work. Peer reviewer reports are available.

Publisher's note: Springer Nature remains neutral with regard to jurisdictional claims in published maps and institutional affiliations.



Open Access This article is licensed under a Creative Commons Attribution 4.0 International License, which permits use, sharing, adaptation, distribution and reproduction in any medium or format, as long as you give appropriate credit to the original author(s) and the source, provide a link to the Creative Commons license, and indicate if changes were made. The images or other third party material in this article are included in the article's Creative Commons license, unless indicated otherwise in a credit line to the material. If material is not included in the article's Creative Commons license and your intended use is not permitted by statutory regulation or exceeds the permitted use, you will need to obtain permission directly from the copyright holder. To view a copy of this license, visit <http://creativecommons.org/licenses/by/4.0/>.

© The Author(s) 2019